Terra Nova

doi: 10.1111/ter.12080

Provenance diversification within an arc-trench system induced by batholith development: the Cretaceous Japan case

Kazumasa Aoki,[1] Yukio Isozaki,[1] Daisuke Kofukuda,[1] Tomohiko Sato,[1] Atsushi Yamamoto,[2] Kenshi Maki,[3] Shuhei Sakata[3] and Takafumi Hirata[3]

[1]*Department of Earth Science and Astronomy, The University of Tokyo, 3-8-1 Komaba, Meguro, Tokyo 153-8902, Japan;* [2]*Department of Life Science, Kinki University, Osaka 577-8502, Japan;* [3]*Department of Geology and Mineralogy, Kyoto University, Kyoto 606-8502, Japan*

ABSTRACT

By comparing detrital zircon U–Pb age spectra of coeval fore-arc and back-/intra-arc basin sandstones, we identified the overall distributary pattern of terrigenous clastic material within the Cretaceous arc system of SW Japan. Abundant Proterozoic (*c.* 1500–2500 Ma) detrital grains from the interior of East Asia are present in the Cretaceous intra-arc basin. However, after a barrier mountain range formed during batholith emplacement, Proterozoic clastics were rarely transported into the fore-arc domain. Episodic batholith formation in Pacific-type orogens likely played a major role in controlling terrigenous supply routes between coeval back-arc and fore-arc domains. The Cretaceous orogen in Japan thus provides a good template for analysing the tectono-sedimentary development of other arc-related basins.

Terra Nova, 26, 139–149, 2014

Introduction

Formation of continental crust during Pacific-type orogeny (Matsuda and Ueda, 1971; Uyeda and Miyashiro, 1974) has occurred along convergent plate margins throughout Earth history. A Pacific-type orogen usually generates the following four major coeval components: (1) an accretionary complex (AC); (2) high-pressure metamorphic rocks (HP-AC); (3) fore-arc basin (FAB) and intra-arc basin (IAB) sediments; and (4) a batholith belt of tonalite–trondjhemite–granodiorite (TTG) (e.g. Maruyama *et al*., 1996; Maruyama, 1997). Of these components, the TTG batholith belt plays the major role in forming juvenile continental crust. However, the surface topography at the time of batholith formation in ancient orogens is commonly obliterated by later tectonics and subsequent surface erosion. In reconstructing the 3-D framework of an ancient Pacific-type orogen, information from arc-related sedimentary basins is invaluable, as demonstrated by the classic studies of the Cordilleran orogen in western North America by Dickinson and Rich (1972), Dickinson and Suczek (1979) and Dickinson *et al*. (1982, 1983). The introduction of detrital zircon geochronology has greatly improved the understanding of Pacific-type orogenic processes and in particular the reconstruction of the tectono-sedimentary development of arc-related basins (e.g. Gehrels *et al*., 2000; Dickinson and Gehrels, 2008a,b; Clift *et al*., 2009; Dumitru *et al*., 2010; Isozaki *et al*., 2010; Aoki *et al*., 2012; LaMaskin, 2012).

The Palaeozoic to Cenozoic basement rocks of Japan formed through multiple episodes of Pacific-type orogeny along the western margin of the Pacific Ocean (e.g. Uyeda and Miyashiro, 1974; Isozaki, 1996; Isozaki *et al*., 2010). In SW Japan, two distinct Cretaceous orogens are a prominent feature of the geological architecture. Both contain the above-mentioned four essential orogenic components and both are still oriented parallel to the arc (e.g. Aoki *et al*., 2011, 2012). However, the terrigenous supply system of each orogen has not been fully documented. To reconstruct the supply system, we compared detrital zircon U–Pb age spectra from Cretaceous sandstones in IABs and FABs from SW Japan by laser-ablation inductively coupled plasma–mass spectrometry (LA-ICPMS). On the basis of these data, we discuss the surface configuration of the growing arc batholith and the relevant changes in terrigenous supply pattern, i.e. the diversification of arc-relevant sedimentary basins.

Correspondence: Kazumasa Aoki, Department of Earth Science and Astronomy, The University of Tokyo, 3-8-1 Komaba, Meguro, Tokyo 153-8902, Japan. Tel: 81-3-5454-6365; e-mail: kazumasa@ea.c.u-tokyo.ac.jp

Geological outline

Two distinct Cretaceous orogens occur in SW Japan: the Late Jurassic–Early Cretaceous Sanbagawa orogen and the mid-Cretaceous–Late Cretaceous Shimanto orogen (e.g. Aoki *et al*., 2011). Each comprises the above-mentioned four major components, i.e. AC, HP-AC, arc batholith and FAB + IAB. In the Sanbagawa orogen, these are the Sanobosan AC, Sanbagawa HP-AC, the Ryoseki-Monobegawa (Rs-Mn) Group (FAB) + Toyonishi Group (IAB) and the Ryoke-Sanyo (Ry-Sy) batholith (Fig. 1). In the Shimanto orogen, they are the Northern Shimanto AC, Shimanto HP-AC, the Izumi Group (FAB) + Kanmon Group (IAB) and the San-in batholith (Fig. 1).

The Sanbosan AC of the Sanbagawa orogen is mainly composed of non- to weakly metamorphosed sandstone and mudstone (trench-fill turbidites) with minor basaltic greenstones of ocean island basalt composition (hotspot-type OIB),

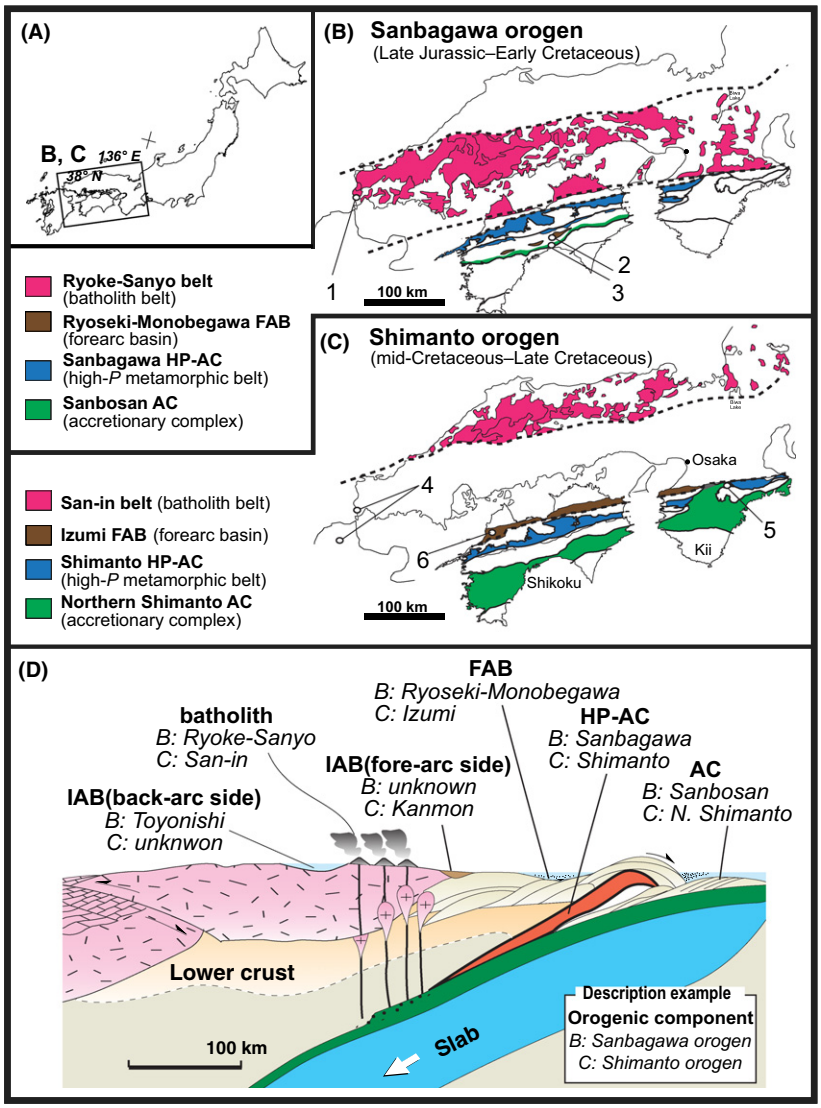

Fig. 1 Spatial distribution of Cretaceous orogens in SW Japan (modified from Aoki *et al.*, 2011). (B, C) Distribution of major orogenic components of the Sanbagawa and Shimanto orogens. As the distribution area of the intra-arc basin (IAB) sediments is small, it is not shown in this figure. Circles show the localities of samples investigated in this study. 1: Toyonishi Group (IAB); 2: Ryoseki-Monobegawa Group (FAB); 3: Sanbosan AC; 4: Kanmon Group (IAB); 5: N. Shimanto AC; 6 Izumi Group (FAB). (D) Schematic illustration of the relative depositional environments at the time of the Sanbagawa and Shimanto orogenies (modified from Maruyama *et al.*, 1996).

non-terrigenous shallow marine limestone (atoll carbonates) and bedded chert (deep-sea pelagic sediments) (Isozaki *et al.*, 1990). The Sanbagawa HP-AC represents the HP-metamorphosed (pumpellyite-actinolite to eclogite facies) part of the Sanbosan AC (Aoki *et al.*, 2009, 2011). The Lower Cretaceous Rs-Mn Group (FAB) consists of non-metamorphosed sandstones/mudstones of shallow marine to non-marine facies (e.g. Suzuki *et al.*, 1990). The uppermost Jurassic to lowest Cretaceous Toyonishi Group is mainly composed of shallow marine-brackish sandstone and mudstone with minor limestone (e.g. Matsumoto, 1949; Yamada and Ohno, 2005; Yoshidomi, 2009). The Ry-Sy batholith comprises Early Cretaceous granite with associated metamorphosed low-*P*–high-*T* older ACs (e.g. Iizumi *et al.*, 1985; Nakajima *et al.*, 1990).

Likewise in the Shimanto orogen, the Northern Shimanto AC is mainly composed of unmetamorphosed turbidites with rare OIBs (Isozaki *et al.*, 1990). The Shimanto HP-AC represents the HP-metamorphosed (pumpellyite-actinolite to epidote–amphibolite facies) part of the Northern Shimanto AC (Aoki *et al.*, 2011). The Izumi Group (FAB) consists of non-metamorphosed turbidites (e.g. Miyata, 1980). The Kanmon Group (IAB) is composed of terrigenous sedimentary rocks with minor pyroclastic rocks (e.g. Matsumoto, 1951; Yamamoto *et al.*, 2009; Yoshidomi, 2009). The San-in batholith consists of Late Cretaceous granites (e.g. Iizumi *et al.*, 1985; Nakajima *et al.*, 1990).

Figure 1(D) shows the original distribution of the above-described Cretaceous orogenic components, constrained by removal of the effect of large-scale Miocene displacement caused by the low-angle thrusting along the older Median Tectonic Line (Isozaki, 1996). The Toyonishi and Kanmon IAB sediments were deposited in back-arc and fore-arc settings respectively.

Analytical procedure

We collected coarse- to medium-grained sandstones from the Toyonishi and Kanmon IABs in SW Japan (Fig. 1), and separated detrital zircons. For the Toyonishi IAB, sandstones were collected from the Kiyosue and Yoshimo formations in ascending order (Matsumoto, 1949). The Kanmon IAB sandstones were collected from the Lower Wakamiya, Shiohama and Sujigahama formations in ascending order (e.g. Yamamoto *et al.*, 2009; Yoshidomi, 2009). The U–Pb age spectrum obtained from the igneous part of the detrital zircons can be used to constrain a change in provenance. Thus, to date the igneous parts of the detrital zircons, the oscillatory-zoned parts of each grain, which are common in igneous zircons (e.g. Corfu *et al.*, 2003), were identified using cathodoluminescence (CL) imaging. We also checked for the presence of mineral inclusions using reflected optical microscopy.

In situ zircon U–Pb dating was carried out using a Nu AtttoM single-collector ICP-MS (Nu instruments,

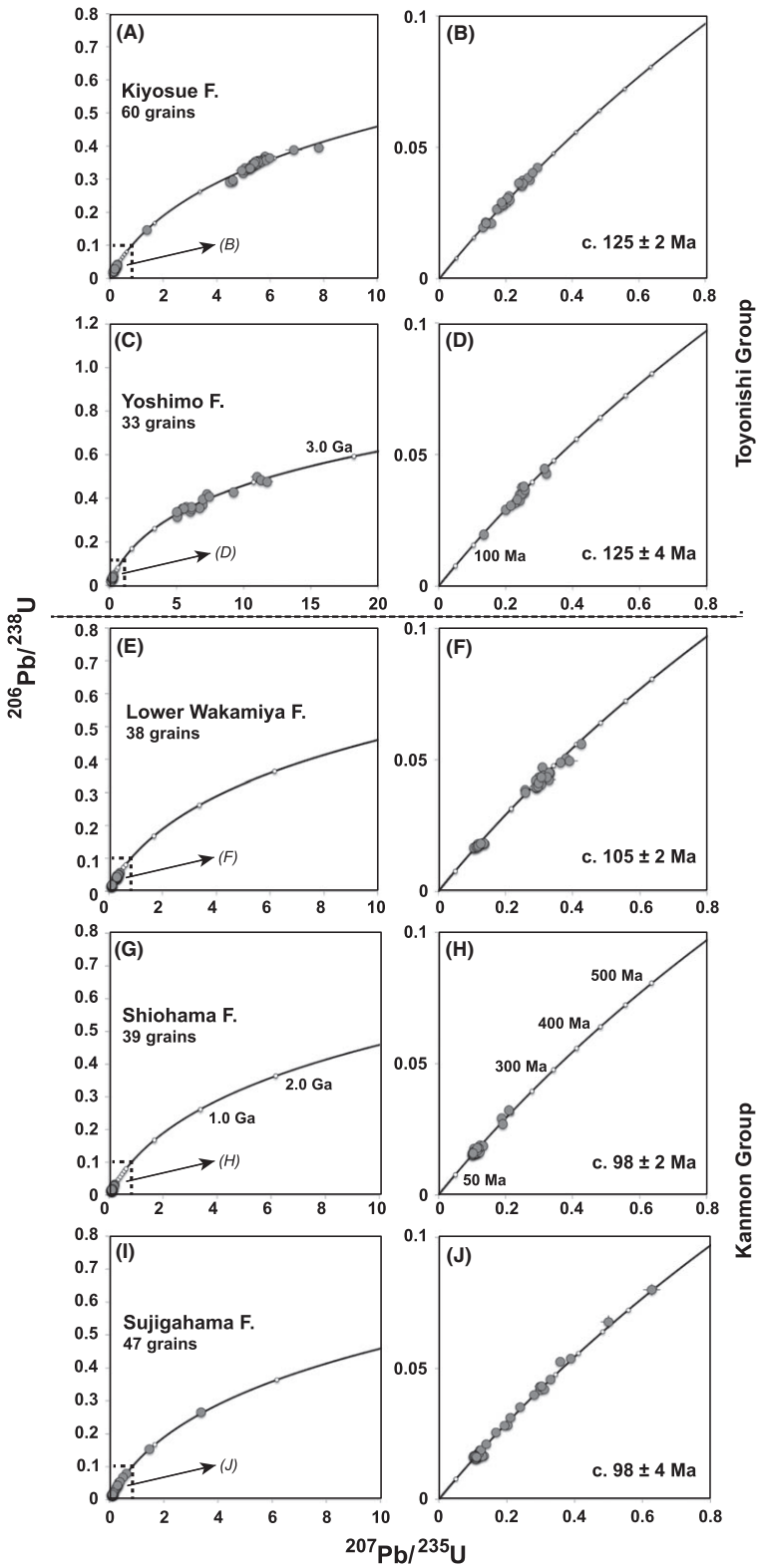

Fig. 2 U–Pb Concordia diagrams for detrital zircons from the Toyonishi Group (A–D) and Kanmon Group (E–J). The Toyonishi Group is composed of the Kiyosue and Yoshimo Formations, and the Kanmon Group of the Lower Wakamiya, Shiohama, and Sujigahama Formations, respectively, in ascending order. The youngest U–Pb age for each formation is also shown in this diagram.

Wrexham, UK) coupled to a NWR-193 laser-ablation system (ESI, Portland, OR, USA), which utilizes a 193-nm ArF excimer laser, at the Department of Geology and Mineralogy, Kyoto University. The laser was operated with an output energy of ~9 mJ per pulse, a repetition rate of 6 or 8 Hz and a laser spot size of 15 μm in diameter, providing an estimated power density of the sample of $<2.72\ Jcm^{-2}$. The pulse counts were 96 or 180 shots. The ICP-MS was optimized using continuous ablation of a 91500 zircon standard (Wiedenbeck *et al.*, 1995, 2004), a NIST SRM 610 and a Plešovice zircon standard (Sláma *et al.*, 2008) to provide maximum sensitivity while maintaining low oxide formation ($UO^+/U^+ < 1\%$). All uncertainties are quoted at the 2 sigma level. ^{235}U was calculated from ^{238}U using a $^{238}U/^{235}U$ ratio of 137.88 (Jaffey *et al.*, 1971). More detailed analytical procedures are given in Iizuka and Hirata (2004) and Hirata *et al.* (2005).

Results

Figure 2 and Tables 1–5 summarize our new zircon U–Pb ages for 217 of 286 grains from the Toyonishi and Kanmon IAB sandstones. Figure 3 shows the $^{206}Pb/^{238}U$ age population of the detrital zircons as probability age frequency curves that were made by *Isoplot/Ex 3* (Ludwig, 2003). To avoid analytical bias owing to lead loss and common lead contamination, obviously discordant measurements from 69 grains were removed. For comparison, we referred to the U–Pb age data for detrital zircons from the Sanbosan and N. Shimanto ACs, and the Rs-Mn and Izumi FAB sandstones (Aoki *et al.*, 2012) (Fig. 3C, D).

In the Sanbagawa orogen, the age frequency curves for the Sanbosan AC, Toyonishi IAB and Rs-Mn FAB sandstones show age clusters between *c.* 100 and 350 Ma (Fig. 3A–D). Notably, the Toyonishi IAB sandstones contain abundant Proterozoic (*c.* 1500–2500 Ma) detrital zircons, in contrast to the other samples.

In the case of the Shimanto orogen, the age frequency curves for the Northern Shimanto AC and the Kanmon IAB sandstones display a

Table 1 Laser-ablation inductively coupled plasma–mass spectrometry isotopic analytical data for detrital zircons from the Kiyosue Fm of the Toyonishi Group.

Grain number	$^{206}Pb/^{238}U$	$^{207}Pb/^{235}U$	$^{207}Pb/^{206}Pb$	Age (Ma)	
				$^{206}Pb/^{238}U$	$^{207}Pb/^{235}U$
1	0.0315 ± 0.00069	0.2087 ± 0.00834	0.0480 ± 0.00161	200.0 ± 4.3	192.4 ± 7.0
2	0.3180 ± 0.00681	4.9980 ± 0.17101	0.1140 ± 0.00304	1780.2 ± 33.4	1819.0 ± 29.4
4	0.3542 ± 0.00755	5.4997 ± 0.18532	0.1126 ± 0.00294	1954.5 ± 36.0	1900.5 ± 29.4
6	0.2925 ± 0.00626	4.6084 ± 0.15736	0.1143 ± 0.00304	1653.9 ± 31.3	1750.8 ± 28.9
7	0.3256 ± 0.00697	5.0531 ± 0.17250	0.1126 ± 0.00299	1816.9 ± 34.0	1828.3 ± 29.4
8	0.3948 ± 0.00142	7.8241 ± 0.20656	0.1437 ± 0.00376	2145.3 ± 6.6	2211.0 ± 24.1
9	0.3459 ± 0.00120	5.4263 ± 0.14284	0.1138 ± 0.00297	1915.2 ± 5.7	1889.0 ± 22.8
10	0.2917 ± 0.00118	4.4935 ± 0.12150	0.1117 ± 0.00299	1650.0 ± 5.9	1729.8 ± 22.7
11	0.3395 ± 0.00124	5.3518 ± 0.14202	0.1143 ± 0.00301	1884.2 ± 6.0	1877.2 ± 23.0
13	0.3391 ± 0.00130	5.3331 ± 0.14264	0.1141 ± 0.00302	1882.5 ± 6.3	1874.2 ± 23.1
15	0.2965 ± 0.00118	4.6112 ± 0.12422	0.1128 ± 0.00301	1673.9 ± 5.9	1751.3 ± 22.7
17	0.0354 ± 0.00014	0.2456 ± 0.00693	0.0503 ± 0.00141	224.4 ± 0.9	223.0 ± 5.7
18	0.3686 ± 0.01463	5.8085 ± 0.33992	0.1143 ± 0.00491	2022.6 ± 69.3	1947.7 ± 52.0
20	0.0354 ± 0.00142	0.2496 ± 0.01645	0.0512 ± 0.00267	224.2 ± 8.9	226.3 ± 13.5
23	0.3317 ± 0.00810	5.2572 ± 0.23007	0.1149 ± 0.00418	1846.7 ± 39.3	1861.9 ± 38.0
25	0.3513 ± 0.00857	5.4429 ± 0.23830	0.1124 ± 0.00408	1940.9 ± 41.0	1891.6 ± 38.3
26	0.0278 ± 0.00068	0.1932 ± 0.00878	0.0503 ± 0.00193	177.1 ± 4.3	179.4 ± 7.5
27	0.0423 ± 0.00104	0.2948 ± 0.01374	0.0505 ± 0.00200	267.4 ± 6.4	262.4 ± 10.8
29	0.3454 ± 0.00842	5.4625 ± 0.23858	0.1147 ± 0.00416	1912.7 ± 40.5	1894.7 ± 38.2
31	0.0291 ± 0.00072	0.2032 ± 0.00962	0.0507 ± 0.00205	184.7 ± 4.5	187.8 ± 8.2
32	0.3313 ± 0.00807	5.1661 ± 0.22510	0.1131 ± 0.00409	1844.5 ± 39.2	1847.0 ± 37.8
33	0.3453 ± 0.00619	5.4316 ± 0.19891	0.1141 ± 0.00364	1912.3 ± 29.7	1889.8 ± 31.9
34	0.3602 ± 0.00646	5.7434 ± 0.21037	0.1156 ± 0.00369	1983.1 ± 30.7	1937.9 ± 32.2
35	0.3572 ± 0.00643	5.6314 ± 0.20824	0.1143 ± 0.00369	1969.1 ± 30.6	1920.9 ± 32.4
36	0.0376 ± 0.00068	0.2719 ± 0.01062	0.0525 ± 0.00182	237.9 ± 4.2	244.2 ± 8.5
37	0.1468 ± 0.00265	1.3946 ± 0.05269	0.0689 ± 0.00229	883.1 ± 14.9	886.6 ± 22.6
38	0.3425 ± 0.00613	5.3911 ± 0.19705	0.1142 ± 0.00364	1898.7 ± 29.5	1883.4 ± 31.8
39	0.0298 ± 0.00054	0.1991 ± 0.00801	0.0485 ± 0.00174	189.3 ± 3.4	184.4 ± 6.8
40	0.0374 ± 0.00069	0.2507 ± 0.01031	0.0485 ± 0.00179	237.0 ± 4.3	227.1 ± 8.4
41	0.0213 ± 0.00041	0.1466 ± 0.00738	0.0500 ± 0.00232	135.7 ± 2.6	138.9 ± 6.6
42	0.0211 ± 0.00047	0.1568 ± 0.01089	0.0539 ± 0.00354	134.7 ± 3.0	147.9 ± 9.6
44	0.0384 ± 0.00076	0.2662 ± 0.00950	0.0503 ± 0.00149	242.7 ± 4.7	239.6 ± 7.7
46	0.3542 ± 0.00678	5.6875 ± 0.14279	0.1164 ± 0.00189	1954.9 ± 32.3	1929.5 ± 21.9
47	0.3501 ± 0.00669	5.5584 ± 0.13913	0.1152 ± 0.00186	1935.0 ± 32.0	1909.7 ± 21.8
48	0.3450 ± 0.00658	5.5052 ± 0.13628	0.1157 ± 0.00183	1910.6 ± 31.6	1901.4 ± 21.5
49	0.3340 ± 0.00643	5.0607 ± 0.13124	0.1099 ± 0.00191	1858.0 ± 31.2	1829.5 ± 22.2
50	0.3512 ± 0.00670	5.6605 ± 0.14005	0.1169 ± 0.00184	1940.1 ± 32.0	1925.4 ± 21.6
51	0.0299 ± 0.00063	0.2118 ± 0.01035	0.0513 ± 0.00226	190.1 ± 4.0	195.0 ± 8.7
52	0.0362 ± 0.00070	0.2514 ± 0.00761	0.0503 ± 0.00117	229.4 ± 4.4	227.7 ± 6.2
53	0.3569 ± 0.00835	5.8387 ± 0.26879	0.1186 ± 0.00470	1967.6 ± 39.8	1952.2 ± 40.7
57	0.0269 ± 0.00065	0.1792 ± 0.00950	0.0484 ± 0.00228	171.0 ± 4.1	167.3 ± 8.2
59	0.3458 ± 0.00808	5.3400 ± 0.24585	0.1120 ± 0.00444	1914.4 ± 38.8	1875.3 ± 40.2
60	0.0306 ± 0.00073	0.2049 ± 0.01070	0.0485 ± 0.00225	194.5 ± 4.6	189.2 ± 9.1
61	0.3881 ± 0.00907	6.8833 ± 0.31684	0.1286 ± 0.00510	2114.0 ± 42.3	2096.5 ± 41.7
63	0.3477 ± 0.00815	5.4007 ± 0.24979	0.1127 ± 0.00449	1923.6 ± 39.1	1885.0 ± 40.4
65	0.3529 ± 0.00824	5.5598 ± 0.25526	0.1143 ± 0.00452	1948.2 ± 39.4	1909.9 ± 40.3
66	0.3533 ± 0.01114	5.4587 ± 0.24629	0.1121 ± 0.00362	1950.2 ± 53.3	1894.1 ± 39.5
67	0.0264 ± 0.00086	0.1731 ± 0.01054	0.0476 ± 0.00244	167.9 ± 5.4	162.1 ± 9.2
68	0.0281 ± 0.00089	0.1900 ± 0.00907	0.0490 ± 0.00175	178.6 ± 5.6	176.6 ± 7.8
69	0.0215 ± 0.00069	0.1396 ± 0.00751	0.0470 ± 0.00203	137.3 ± 4.4	132.7 ± 6.7
72	0.3480 ± 0.01098	5.4086 ± 0.24456	0.1127 ± 0.00365	1924.8 ± 52.7	1886.2 ± 39.5
73	0.0364 ± 0.00116	0.2395 ± 0.01215	0.0477 ± 0.00188	230.4 ± 7.2	218.0 ± 10.0
75	0.0403 ± 0.00127	0.2807 ± 0.01309	0.0506 ± 0.00173	254.4 ± 7.9	251.2 ± 10.4
76	0.3315 ± 0.00531	5.2146 ± 0.23197	0.1141 ± 0.00473	1845.7 ± 25.8	1855.0 ± 38.6
77	0.0195 ± 0.00034	0.1314 ± 0.00722	0.0488 ± 0.00254	124.6 ± 2.1	125.4 ± 6.5
78	0.3327 ± 0.00537	5.2484 ± 0.23560	0.1144 ± 0.00479	1851.5 ± 26.0	1860.5 ± 39.0
80	0.0211 ± 0.00039	0.1400 ± 0.00877	0.0482 ± 0.00288	134.5 ± 2.5	133.0 ± 7.8

Table 1 (Continued).

Grain number	$^{206}Pb/^{238}U$	$^{207}Pb/^{235}U$	$^{207}Pb/^{206}Pb$	Age (Ma) $^{206}Pb/^{238}U$	Age (Ma) $^{207}Pb/^{235}U$
82	0.3260 ± 0.00525	4.9386 ± 0.22112	0.1099 ± 0.00459	1818.8 ± 25.6	1808.9 ± 38.5
84	0.3640 ± 0.00583	5.9848 ± 0.26598	0.1193 ± 0.00494	2001.0 ± 27.6	1973.6 ± 39.4
85	0.0291 ± 0.00048	0.1873 ± 0.00893	0.0467 ± 0.00209	184.8 ± 3.0	174.3 ± 7.7

All errors are quoted at 2σ.

Table 2 Laser-ablation inductively coupled plasma–mass spectrometry isotopic analytical data for detrital zircons from the Yoshimo Fm of the Toyonishi Group.

Grain number	$^{206}Pb/^{238}U$	$^{207}Pb/^{235}U$	$^{207}Pb/^{206}Pb$	Age (Ma) $^{206}Pb/^{238}U$	Age (Ma) $^{207}Pb/^{235}U$
Yo-1	0.4183 ± 0.01544	7.2644 ± 0.32279	0.1260 ± 0.00165	2252.8 ± 98.8	2144.5 ± 284.0
Yo-2	0.3381 ± 0.01250	6.0525 ± 0.28285	0.1299 ± 0.00183	1877.3 ± 80.1	1983.4 ± 252.9
Yo-3	0.0347 ± 0.00131	0.2417 ± 0.01332	0.0505 ± 0.00171	220.1 ± 8.5	219.8 ± 13.4
Yo-4	0.0376 ± 0.00144	0.2484 ± 0.01541	0.0480 ± 0.00201	237.8 ± 9.3	225.3 ± 15.5
Yo-5	0.3932 ± 0.01450	6.1857 ± 0.26668	0.1141 ± 0.00145	2137.8 ± 92.8	2002.4 ± 240.0
Yo-6	0.3711 ± 0.01369	6.9532 ± 0.30433	0.1359 ± 0.00175	2034.3 ± 87.7	2105.5 ± 269.8
Yo-7	0.0354 ± 0.00133	0.2555 ± 0.01319	0.0524 ± 0.00153	224.1 ± 8.6	231.0 ± 13.3
Yo-8	0.3597 ± 0.01331	5.7344 ± 0.26855	0.1156 ± 0.00164	1981.0 ± 85.2	1936.6 ± 241.5
Yo-9	0.4983 ± 0.01838	11.0131 ± 0.47779	0.1603 ± 0.00202	2606.6 ± 117.4	2524.2 ± 396.6
Yo-12	0.3559 ± 0.00783	6.7321 ± 0.20243	0.1372 ± 0.00200	1962.9 ± 50.3	2076.8 ± 187.2
Yo-14	0.3519 ± 0.00773	5.4468 ± 0.15676	0.1123 ± 0.00162	1943.7 ± 49.6	1892.2 ± 147.9
Yo-15	0.3950 ± 0.00867	6.9476 ± 0.19879	0.1276 ± 0.00182	2146.0 ± 55.7	2104.8 ± 184.1
Yo-18	0.0196 ± 0.00054	0.1354 ± 0.00954	0.0501 ± 0.00317	125.2 ± 3.5	129.0 ± 9.6
Yo-22	0.0317 ± 0.00080	0.2294 ± 0.01312	0.0525 ± 0.00249	201.2 ± 5.2	209.7 ± 13.2
Yo-25	0.3344 ± 0.00608	5.1102 ± 0.16410	0.1108 ± 0.00228	1859.9 ± 39.1	1837.8 ± 154.3
Yo-27	0.4078 ± 0.00749	7.4576 ± 0.27547	0.1327 ± 0.00280	2204.6 ± 48.1	2167.9 ± 247.1
Yo-28	0.0326 ± 0.00070	0.2424 ± 0.01339	0.0539 ± 0.00251	207.0 ± 4.5	220.4 ± 13.5
Yo-30	0.3493 ± 0.00635	6.1401 ± 0.19787	0.1275 ± 0.00262	1931.1 ± 40.8	1996.0 ± 183.3
Yo-32	0.0351 ± 0.00068	0.2484 ± 0.01033	0.0514 ± 0.00173	222.3 ± 4.4	225.3 ± 10.4
Yo-34	0.0328 ± 0.00062	0.2348 ± 0.00822	0.0518 ± 0.00142	208.3 ± 4.0	214.2 ± 8.3
Yo-37	0.0290 ± 0.00087	0.1998 ± 0.00834	0.0500 ± 0.00135	184.1 ± 5.6	185.0 ± 8.4
Yo-41	0.0306 ± 0.00096	0.2148 ± 0.01226	0.0509 ± 0.00225	194.3 ± 6.2	197.6 ± 12.4
Yo-42	0.4275 ± 0.01263	9.2505 ± 0.38049	0.1570 ± 0.00296	2294.3 ± 80.9	2363.1 ± 327.4
Yo-43	0.3149 ± 0.00929	5.0607 ± 0.19922	0.1166 ± 0.00221	1764.7 ± 59.6	1829.5 ± 184.5
Yo-44	0.0428 ± 0.00129	0.3219 ± 0.01420	0.0545 ± 0.00157	270.2 ± 8.3	283.4 ± 14.3
Yo-45	0.3589 ± 0.01062	6.1258 ± 0.25766	0.1238 ± 0.00241	1977.0 ± 68.1	1993.9 ± 232.8
Yo-46	0.4829 ± 0.01444	11.2965 ± 0.59648	0.1697 ± 0.00350	2540.1 ± 92.4	2547.9 ± 475.0
Yo-47	0.3530 ± 0.00455	5.5508 ± 0.11348	0.1140 ± 0.00240	1948.8 ± 29.2	1908.5 ± 109.1
Yo-48	0.0446 ± 0.00068	0.3161 ± 0.01234	0.0514 ± 0.00191	281.3 ± 4.4	278.9 ± 12.5
Yo-49	0.3371 ± 0.00459	5.0363 ± 0.17284	0.1083 ± 0.00254	1872.6 ± 29.6	1825.5 ± 161.9
Yo-51	0.4767 ± 0.00652	11.7460 ± 0.44192	0.1786 ± 0.00400	2513.0 ± 41.9	2584.4 ± 371.6
Yo-52	0.0366 ± 0.00065	0.2573 ± 0.01387	0.0510 ± 0.00256	231.7 ± 4.2	232.5 ± 14.0
Yo-53	0.0378 ± 0.00072	0.2542 ± 0.01555	0.0488 ± 0.00275	239.1 ± 4.6	230.0 ± 15.7

All errors are quoted at 2σ.

prominent U–Pb age cluster between c. 80 and 350 Ma. There was no significant difference among the age frequency curves for the sandstones from the three formations of the Kanmon Group. The age frequency curve for the Izumi FAB sandstone shows age clusters at *c.* 80–120 Ma (Fig. 3I). However, the Northern Shimanto AC sandstones display a broader age spectrum with grains aged between *c.* 1500 and 3000 Ma.

Discussion

The presence of Permian–Cretaceous detrital zircons, together with Proterozoic zircons, in the sandstones provides significant information regarding the terrigenous supply system in the Cretaceous orogen of Japan. First, terrigenous clastics were supplied from Permian–Cretaceous juvenile crust ubiquitously to the Cretaceous FAB and IAB. Second, most of the Proterozoic clastics from

Table 3 Laser-ablation inductively coupled plasma–mass spectrometry isotopic analytical data for detrital zircons from the Lower Wakamiya Fm of the Kanmon Group.

				Age (Ma)	
Grain number	$^{206}Pb/^{238}U$	$^{207}Pb/^{235}U$	$^{207}Pb/^{206}Pb$	$^{206}Pb/^{238}U$	$^{207}Pb/^{235}U$
WA-1	0.0178 ± 0.00063	0.1162 ± 0.00736	0.0474 ± 0.00257	113.7 ± 4.0	111.7 ± 7.5
WA-3	0.0386 ± 0.00132	0.2581 ± 0.01495	0.0485 ± 0.00217	243.9 ± 8.5	233.1 ± 15.1
WA-4	0.0419 ± 0.00147	0.3041 ± 0.01979	0.0526 ± 0.00267	264.5 ± 9.5	269.6 ± 19.9
WA-5	0.0432 ± 0.00149	0.2989 ± 0.01804	0.0501 ± 0.00232	272.9 ± 9.6	265.6 ± 18.2
WA-6	0.0470 ± 0.00157	0.3106 ± 0.01504	0.0479 ± 0.00163	296.1 ± 10.1	274.7 ± 15.2
WA-7	0.0421 ± 0.00138	0.2907 ± 0.01178	0.0501 ± 0.00129	265.7 ± 8.9	259.1 ± 11.9
WA-8	0.0179 ± 0.00063	0.1208 ± 0.00755	0.0489 ± 0.00260	114.5 ± 4.1	115.8 ± 7.6
WA-9	0.0436 ± 0.00065	0.3110 ± 0.01418	0.0517 ± 0.00203	275.4 ± 4.2	275.0 ± 14.3
WA-11	0.0430 ± 0.00055	0.3054 ± 0.00976	0.0515 ± 0.00144	271.6 ± 3.5	270.6 ± 9.9
WA-12	0.0439 ± 0.00054	0.3127 ± 0.00879	0.0516 ± 0.00127	277.1 ± 3.5	276.3 ± 8.9
WA-13	0.0377 ± 0.00060	0.2596 ± 0.01323	0.0499 ± 0.00225	238.6 ± 3.9	234.3 ± 13.3
WA-14	0.0560 ± 0.00072	0.4257 ± 0.01408	0.0551 ± 0.00152	351.5 ± 4.6	360.1 ± 14.2
WA-15	0.0393 ± 0.00055	0.2925 ± 0.01166	0.0540 ± 0.00188	248.6 ± 3.6	260.5 ± 11.8
WA-16	0.0173 ± 0.00028	0.1148 ± 0.00556	0.0480 ± 0.00223	110.8 ± 1.8	110.4 ± 5.6
WA-17	0.0165 ± 0.00031	0.1107 ± 0.00677	0.0488 ± 0.00286	105.2 ± 2.0	106.6 ± 6.9
WA-18	0.0397 ± 0.00123	0.2911 ± 0.01455	0.0532 ± 0.00182	251.1 ± 7.9	259.4 ± 14.7
WA-19	0.0407 ± 0.00125	0.3072 ± 0.01432	0.0548 ± 0.00165	257.0 ± 8.0	272.0 ± 14.4
WA-20	0.0400 ± 0.00128	0.2965 ± 0.01805	0.0538 ± 0.00245	252.7 ± 8.3	263.7 ± 18.2
WA-21	0.0167 ± 0.00061	0.1057 ± 0.00986	0.0460 ± 0.00388	106.6 ± 3.9	102.0 ± 10.0
WA-22	0.0424 ± 0.00136	0.3293 ± 0.02005	0.0563 ± 0.00253	267.7 ± 8.8	289.0 ± 20.2
WA-23	0.0180 ± 0.00059	0.1186 ± 0.00778	0.0478 ± 0.00263	114.9 ± 3.8	113.8 ± 7.9
WA-24	0.0411 ± 0.00126	0.2983 ± 0.01374	0.0526 ± 0.00156	259.9 ± 8.1	265.0 ± 13.9
WA-25	0.0180 ± 0.00057	0.1382 ± 0.00737	0.0556 ± 0.00227	115.3 ± 3.7	131.5 ± 7.5
WA-26	0.0177 ± 0.00062	0.1229 ± 0.00995	0.0504 ± 0.00359	113.0 ± 4.0	117.7 ± 10.1
WA-27	0.0449 ± 0.00065	0.3328 ± 0.01289	0.0537 ± 0.00173	283.3 ± 4.2	291.7 ± 13.0
WA-29	0.0169 ± 0.00028	0.1132 ± 0.00565	0.0485 ± 0.00226	108.2 ± 1.8	108.9 ± 5.7
WA-30	0.0504 ± 0.00069	0.3806 ± 0.01295	0.0548 ± 0.00151	316.9 ± 4.4	327.4 ± 13.1
WA-31	0.0184 ± 0.00047	0.1314 ± 0.01176	0.0518 ± 0.00438	117.6 ± 3.0	125.4 ± 11.9
WA-32	0.0183 ± 0.00030	0.1357 ± 0.00649	0.0537 ± 0.00237	117.1 ± 2.0	129.2 ± 6.6
WA-33	0.0451 ± 0.00060	0.3308 ± 0.01011	0.0532 ± 0.00132	284.5 ± 3.8	290.2 ± 10.2
WA-34	0.0495 ± 0.00095	0.3902 ± 0.02536	0.0572 ± 0.00307	311.4 ± 6.1	334.5 ± 25.4
WA-35	0.0490 ± 0.00062	0.3646 ± 0.00982	0.0540 ± 0.00115	308.1 ± 4.0	315.6 ± 9.9
WA-36	0.0433 ± 0.00082	0.3244 ± 0.01866	0.0543 ± 0.00267	273.5 ± 5.3	285.3 ± 18.8
WA-37	0.0433 ± 0.00081	0.3070 ± 0.01748	0.0514 ± 0.00252	273.2 ± 5.2	271.9 ± 17.6
WA-39	0.0169 ± 0.00034	0.1173 ± 0.00709	0.0503 ± 0.00283	108.2 ± 2.2	112.6 ± 7.2
WA-40	0.0175 ± 0.00037	0.1194 ± 0.00805	0.0496 ± 0.00313	111.5 ± 2.4	114.5 ± 8.1
WA-41	0.0182 ± 0.00038	0.1264 ± 0.00815	0.0503 ± 0.00302	116.4 ± 2.4	120.8 ± 8.2

All errors are quoted at 2σ.

older continental basements were deposited in the Cretaceous back-arc domain, with few older clastics delivered to the coeval fore-arc.

Sandstones deposited in arc-related basins within a Pacific-type orogen normally contain large amounts of terrigenous clastics that were derived directly from adjacent arc crust containing coeval volcanics and slightly older granitoid batholiths, as well as older continental margin rocks. The occurrence of rare Cambrian-Ordovician zircons indicates the exposure/erosion of older arc crust that is consistent with the overall tectonic framework of the Pacific-type orogen in Japan since *c*. 500 Ma (Cambrian) (e.g. Isozaki *et al*., 2010).

In an ordinary subduction-related Pacific-type orogen, volcanic arcs develop usually *c*. ~200 km away from the contemporary trench, forming a prominent topographic relief that divides back-arc and fore-arc domains. Juvenile arc volcanic rocks in this environment become the main source of clastics, whereas coeval TTG rocks of the underlying batholith will be exposed after the successive surface uplift and erosion. The thickening of arc crust by successive periods of arc magmatism adds buoyancy to induce the surface uplift of the arc crust. By removing the covering volcanic edifice through selective periods of erosion, deep-seated batholith rocks are eventually exposed on the surface. As soon as the TTG batholith is exposed, abundant terrigenous clastics with zircons from the TTG batholith are supplied to both sides of the arc (Fig. 4). The Cretaceous arc-related basins in SW Japan obviously record such a sequence of processes (Isozaki *et al*., 2010; Aoki *et al*., 2012; present study).

We have identified a unique zircon population with abundant Proterozoic grains in the Toyonishi IAB

Table 4 Laser-ablation inductively coupled plasma–mass spectrometry isotopic analytical data for detrital zircons from the Shiohama Fm of the Kanmon Group.

				Age (Ma)	
Grain number	$^{206}Pb/^{238}U$	$^{207}Pb/^{235}U$	$^{207}Pb/^{206}Pb$	$^{206}Pb/^{238}U$	$^{207}Pb/^{235}U$
SHI-1	0.0171 ± 0.00040	0.1075 ± 0.00627	0.0456 ± 0.00248	109.2 ± 2.6	103.7 ± 6.3
SHI-2	0.0323 ± 0.00067	0.2104 ± 0.00825	0.0473 ± 0.00162	204.8 ± 4.3	193.9 ± 8.3
SHI-3	0.0161 ± 0.00038	0.1186 ± 0.00681	0.0534 ± 0.00284	103.1 ± 2.5	113.8 ± 6.9
SHI-5	0.0153 ± 0.00034	0.1007 ± 0.00493	0.0477 ± 0.00215	98.1 ± 2.2	97.5 ± 5.0
SHI-6	0.0291 ± 0.00061	0.1883 ± 0.00760	0.0469 ± 0.00166	184.9 ± 3.9	175.2 ± 7.7
SHI-7	0.0160 ± 0.00034	0.1101 ± 0.00453	0.0499 ± 0.00185	102.3 ± 2.2	106.1 ± 4.6
SHI-8	0.0157 ± 0.00036	0.1040 ± 0.00581	0.0480 ± 0.00249	100.6 ± 2.3	100.5 ± 5.9
SHI-9	0.0176 ± 0.00038	0.1064 ± 0.00516	0.0439 ± 0.00195	112.2 ± 2.5	102.6 ± 5.2
SHI-10	0.0155 ± 0.00025	0.1011 ± 0.00525	0.0474 ± 0.00224	99.0 ± 1.6	97.8 ± 5.3
SHI-12	0.0165 ± 0.00021	0.1106 ± 0.00410	0.0487 ± 0.00154	105.3 ± 1.4	106.5 ± 4.2
SHI-13	0.0164 ± 0.00034	0.1049 ± 0.00798	0.0464 ± 0.00330	104.8 ± 2.2	101.3 ± 8.1
SHI-14	0.0270 ± 0.00032	0.1917 ± 0.00585	0.0515 ± 0.00121	171.8 ± 2.0	178.1 ± 5.9
SHI-15	0.0160 ± 0.00023	0.1042 ± 0.00460	0.0473 ± 0.00185	102.2 ± 1.5	100.7 ± 4.7
SHI-16	0.0165 ± 0.00028	0.1148 ± 0.00650	0.0503 ± 0.00260	105.8 ± 1.8	110.3 ± 6.6
SHI-18	0.0161 ± 0.00036	0.1082 ± 0.00544	0.0487 ± 0.00236	103.1 ± 2.3	104.3 ± 5.5
SHI-20	0.0165 ± 0.00038	0.1117 ± 0.00602	0.0490 ± 0.00254	105.7 ± 2.5	107.5 ± 6.1
SHI-21	0.0165 ± 0.00039	0.1089 ± 0.00631	0.0478 ± 0.00267	105.7 ± 2.5	105.0 ± 6.4
SHI-22	0.0169 ± 0.00038	0.1166 ± 0.00550	0.0500 ± 0.00227	108.0 ± 2.4	112.0 ± 5.6
SHI-24	0.0167 ± 0.00041	0.1174 ± 0.00714	0.0510 ± 0.00298	106.7 ± 2.6	112.7 ± 7.2
SHI-25	0.0174 ± 0.00042	0.1194 ± 0.00695	0.0496 ± 0.00277	111.5 ± 2.7	114.6 ± 7.0
SHI-30	0.0168 ± 0.00058	0.1110 ± 0.00588	0.0479 ± 0.00181	107.6 ± 3.7	106.9 ± 6.0
SHI-31	0.0165 ± 0.00058	0.1056 ± 0.00637	0.0465 ± 0.00218	105.4 ± 3.7	101.9 ± 6.4
SHI-32	0.0159 ± 0.00056	0.1110 ± 0.00672	0.0507 ± 0.00240	101.5 ± 3.6	106.9 ± 6.8
SHI-33	0.0168 ± 0.00061	0.1127 ± 0.00823	0.0488 ± 0.00299	107.1 ± 4.0	108.5 ± 8.3
SHI-34	0.0183 ± 0.00063	0.1210 ± 0.00632	0.0478 ± 0.00176	117.2 ± 4.1	116.0 ± 6.4
SHI-35	0.0165 ± 0.00058	0.1131 ± 0.00648	0.0496 ± 0.00214	105.7 ± 3.7	108.8 ± 6.6
SHI-37	0.0160 ± 0.00032	0.1010 ± 0.00486	0.0459 ± 0.00218	102.0 ± 2.1	97.7 ± 4.9
SHI-38	0.0172 ± 0.00043	0.1203 ± 0.00899	0.0507 ± 0.00366	110.0 ± 2.8	115.3 ± 9.1
SHI-40	0.0159 ± 0.00032	0.1118 ± 0.00528	0.0511 ± 0.00237	101.5 ± 2.1	107.7 ± 5.3
SHI-41	0.0174 ± 0.00034	0.1157 ± 0.00527	0.0482 ± 0.00215	111.3 ± 2.2	111.2 ± 5.3
SHI-42	0.0189 ± 0.00041	0.1238 ± 0.00711	0.0475 ± 0.00264	120.7 ± 2.6	118.5 ± 7.2
SHI-43	0.0187 ± 0.00037	0.1336 ± 0.00594	0.0517 ± 0.00224	119.7 ± 2.4	127.4 ± 6.0
SHI-45	0.0164 ± 0.00033	0.1039 ± 0.00520	0.0459 ± 0.00225	105.0 ± 2.1	100.4 ± 5.3
SHI-46	0.0164 ± 0.00043	0.1227 ± 0.00672	0.0541 ± 0.00307	105.0 ± 2.7	117.5 ± 6.8
SHI-47	0.0178 ± 0.00044	0.1212 ± 0.00582	0.0495 ± 0.00251	113.5 ± 2.8	116.2 ± 5.9
SHI-48	0.0169 ± 0.00043	0.1151 ± 0.00614	0.0492 ± 0.00273	108.3 ± 2.8	110.6 ± 6.2
SHI-49	0.0170 ± 0.00041	0.1165 ± 0.00523	0.0498 ± 0.00240	108.4 ± 2.7	111.9 ± 5.3
SHI-53	0.0179 ± 0.00046	0.1162 ± 0.00657	0.0470 ± 0.00274	114.3 ± 3.0	111.6 ± 6.7
SHI-54	0.0158 ± 0.00037	0.1034 ± 0.00392	0.0473 ± 0.00200	101.2 ± 2.4	99.9 ± 4.0

All errors are quoted at 2σ.

sandstone in the Sanbagawa orogen (Fig. 3). The Proterozoic zircons were mostly supplied to the Toyonishi IAB rather than to the fore-arc domains (Sanbosan AC and Rs-Mn FAB). Potential provenances with Proterozoic basements in East Asia adjacent to Japan, which could provide detrital grains to Cretaceous Japan, are the North and South China blocks (e.g. Jin, 2002; Darby and Gehrels, 2006; Liu *et al.*, 2008; Wang *et al.*, 2010; Xu *et al.*, 2014; Zhu *et al.*, 2014). This is because post-Triassic Japan evolved along the eastern margin of the amalgamated South and North China blocks (e.g. Maruyama *et al.*, 1989, 1997; Isozaki, 1996; Isozaki *et al.*, 2010). The Proterozoic zircons were likely transported from the interior of Early Cretaceous East Asia into the Toyonishi IAB (Fig. 4).

The Jurassic AC in Japan also contains abundant Proterozoic clasts, i.e. boulders of gneiss/granite, and detrital grains of zircons and monazites (e.g. Shibata and Adachi, 1974; Suzuki *et al.*, 1991; Nutman *et al.*, 2006). Therefore, the Proterozoic zircons detected in the Toyonishi IAB sandstones could possibly be derived from already exposed parts of the Jurassic AC in the Cretaceous back-arc region (Fig. 4).

In contrast, it is noteworthy that the Proterozoic zircons are quite rare in the coeval Sanbosan AC and Rs-Mn FAB sandstones. This contrast between the IAB and FAB sandstones indicates that the ordinary oceanward terrigenous supply of continental clastics was aborted somewhere in the middle of the Cretaceous arc. The uplifted Cretaceous Ry-Sy

Table 5 Laser-ablation inductively coupled plasma–mass spectrometry isotopic analytical data for detrital zircons from the Sujigahama Fm of the Kanmon Group.

Grain number	$^{206}Pb/^{238}U$	$^{207}Pb/^{235}U$	$^{207}Pb/^{206}Pb$	Age (Ma)	
				$^{206}Pb/^{238}U$	$^{207}Pb/^{235}U$
SJ-2	0.0458 ± 0.00103	0.3286 ± 0.00845	0.0520 ± 0.00114	288.8 ± 6.6	288.5 ± 8.5
SJ-3	0.1540 ± 0.00343	1.4662 ± 0.03613	0.0690 ± 0.00117	923.4 ± 22.1	916.6 ± 36.0
SJ-4	0.0169 ± 0.00040	0.1138 ± 0.00440	0.0489 ± 0.00179	107.9 ± 2.6	109.4 ± 4.5
SJ-5	0.0176 ± 0.00042	0.1157 ± 0.00486	0.0476 ± 0.00189	112.6 ± 2.7	111.2 ± 4.9
SJ-6	0.0188 ± 0.00046	0.1210 ± 0.00546	0.0468 ± 0.00199	119.8 ± 2.9	116.0 ± 5.5
SJ-7	0.0185 ± 0.00044	0.1231 ± 0.00489	0.0482 ± 0.00180	118.4 ± 2.8	117.9 ± 4.9
SJ-8	0.0283 ± 0.00064	0.2025 ± 0.00538	0.0519 ± 0.00123	180.0 ± 4.1	187.2 ± 5.4
SJ-9	0.0173 ± 0.00042	0.1226 ± 0.00515	0.0513 ± 0.00204	110.7 ± 2.7	117.4 ± 5.2
SJ-10	0.0526 ± 0.00146	0.3575 ± 0.01423	0.0493 ± 0.00114	330.4 ± 9.4	310.4 ± 14.4
SJ-11	0.0157 ± 0.00049	0.1114 ± 0.00753	0.0515 ± 0.00299	100.3 ± 3.2	107.3 ± 7.6
SJ-12	0.0163 ± 0.00050	0.1081 ± 0.00696	0.0482 ± 0.00263	104.0 ± 3.2	104.2 ± 7.0
SJ-13	0.0160 ± 0.00050	0.1191 ± 0.00779	0.0540 ± 0.00300	102.4 ± 3.2	114.3 ± 7.9
SJ-14	0.0800 ± 0.00221	0.6267 ± 0.02502	0.0568 ± 0.00128	496.1 ± 14.3	494.0 ± 25.1
SJ-15	0.0417 ± 0.00116	0.2983 ± 0.01233	0.0518 ± 0.00132	263.6 ± 7.5	265.0 ± 12.4
SJ-17	0.0182 ± 0.00051	0.1200 ± 0.00525	0.0479 ± 0.00144	116.0 ± 3.3	115.1 ± 5.3
SJ-18	0.0165 ± 0.00048	0.1063 ± 0.00552	0.0469 ± 0.00189	105.2 ± 3.1	102.6 ± 5.6
SJ-20	0.0165 ± 0.00066	0.1156 ± 0.00671	0.0508 ± 0.00196	105.6 ± 4.3	111.0 ± 6.8
SJ-21	0.0399 ± 0.00158	0.2808 ± 0.01505	0.0511 ± 0.00154	252.0 ± 10.2	251.3 ± 15.2
SJ-22	0.0255 ± 0.00101	0.1680 ± 0.00898	0.0478 ± 0.00149	162.2 ± 6.5	157.6 ± 9.1
SJ-23	0.0166 ± 0.00068	0.1028 ± 0.00682	0.0449 ± 0.00222	106.2 ± 4.4	99.4 ± 6.9
SJ-24	0.0312 ± 0.00123	0.2110 ± 0.01091	0.0490 ± 0.00138	198.3 ± 8.0	194.4 ± 11.0
SJ-25	0.0161 ± 0.00065	0.1093 ± 0.00692	0.0492 ± 0.00224	103.0 ± 4.2	105.3 ± 7.0
SJ-26	0.0168 ± 0.00069	0.1085 ± 0.00733	0.0468 ± 0.00238	107.6 ± 4.4	104.6 ± 7.4
SJ-27	0.0171 ± 0.00071	0.1166 ± 0.00849	0.0494 ± 0.00281	109.4 ± 4.6	112.0 ± 8.6
SJ-28	0.0282 ± 0.00104	0.1933 ± 0.00985	0.0498 ± 0.00165	179.0 ± 6.7	179.4 ± 10.0
SJ-29	0.0678 ± 0.00248	0.4996 ± 0.02240	0.0534 ± 0.00125	422.9 ± 16.0	411.4 ± 22.5
SJ-30	0.0162 ± 0.00064	0.1014 ± 0.00742	0.0453 ± 0.00277	103.8 ± 4.1	98.0 ± 7.5
SJ-32	0.0156 ± 0.00059	0.1059 ± 0.00624	0.0492 ± 0.00219	99.9 ± 3.8	102.3 ± 6.3
SJ-34	0.0154 ± 0.00057	0.1101 ± 0.00584	0.0519 ± 0.00192	98.3 ± 3.7	106.0 ± 5.9
SJ-35	0.0352 ± 0.00129	0.2391 ± 0.01093	0.0493 ± 0.00127	222.8 ± 8.3	217.7 ± 11.0
SJ-36	0.0166 ± 0.00063	0.1329 ± 0.00766	0.0579 ± 0.00247	106.3 ± 4.1	126.7 ± 7.7
SJ-37	0.2660 ± 0.00279	3.3718 ± 0.12305	0.0919 ± 0.00205	1520.6 ± 18.0	1497.9 ± 117.8
SJ-38	0.0167 ± 0.00021	0.1130 ± 0.00446	0.0492 ± 0.00188	106.5 ± 1.4	108.7 ± 4.5
SJ-39	0.0165 ± 0.00025	0.1279 ± 0.00610	0.0562 ± 0.00258	105.5 ± 1.6	122.2 ± 6.2
SJ-40	0.0175 ± 0.00021	0.1182 ± 0.00442	0.0489 ± 0.00177	111.9 ± 1.4	113.4 ± 4.5
SJ-41	0.0187 ± 0.00021	0.1237 ± 0.00414	0.0480 ± 0.00155	119.4 ± 1.4	118.5 ± 4.2
SJ-42	0.0421 ± 0.00047	0.3101 ± 0.01019	0.0534 ± 0.00159	265.7 ± 3.0	274.3 ± 10.3
SJ-43	0.0161 ± 0.00027	0.1093 ± 0.00646	0.0492 ± 0.00281	103.0 ± 1.8	105.3 ± 6.5
SJ-44	0.0167 ± 0.00020	0.1069 ± 0.00376	0.0466 ± 0.00159	106.5 ± 1.3	103.2 ± 3.8
SJ-45	0.0538 ± 0.00052	0.3886 ± 0.00940	0.0524 ± 0.00117	337.7 ± 3.4	333.3 ± 9.5
SJ-46	0.0158 ± 0.00031	0.1103 ± 0.00706	0.0507 ± 0.00309	100.8 ± 2.0	106.2 ± 7.1
SJ-47	0.0164 ± 0.00031	0.1039 ± 0.00648	0.0460 ± 0.00273	104.8 ± 2.0	100.3 ± 6.6
SJ-49	0.0165 ± 0.00023	0.1071 ± 0.00415	0.0472 ± 0.00170	105.2 ± 1.5	103.3 ± 4.2
SJ-51	0.0431 ± 0.00071	0.2981 ± 0.01606	0.0502 ± 0.00233	271.9 ± 4.6	264.9 ± 16.2
SJ-52	0.0432 ± 0.00071	0.3026 ± 0.01594	0.0508 ± 0.00230	272.7 ± 4.6	268.4 ± 16.1
SJ-53	0.0211 ± 0.00028	0.1394 ± 0.00451	0.0480 ± 0.00140	134.5 ± 1.8	132.5 ± 4.6
SJ-54	0.0161 ± 0.00032	0.1114 ± 0.00738	0.0501 ± 0.00316	103.2 ± 2.1	107.3 ± 7.5

All errors are quoted at 2σ.

batholith belt likely acted not only as the main provenance, but also as an efficient barrier that prevented the direct delivery of the Proterozoic continental clastics to the active trench through surface transportation during the Late Jurassic–Early Cretaceous Sanbagawa orogeny.

Likewise in the case of the mid-Cretaceous–Late Cretaceous Shimanto orogen, the sandstones in the fore-arc (N. Shimanto AC, Izumi FAB and Kanmon IAB) contain significantly fewer Proterozoic zircons. Although IAB sandstones in the back-arc have not yet been recognized in the Shimanto orogen, the Late Cretaceous San-in batholith also likely acted as an efficient barrier that prevented the direct delivery of continent-derived terrigenous clastics.

Comparing the zircon age data from the two sets of Cretaceous

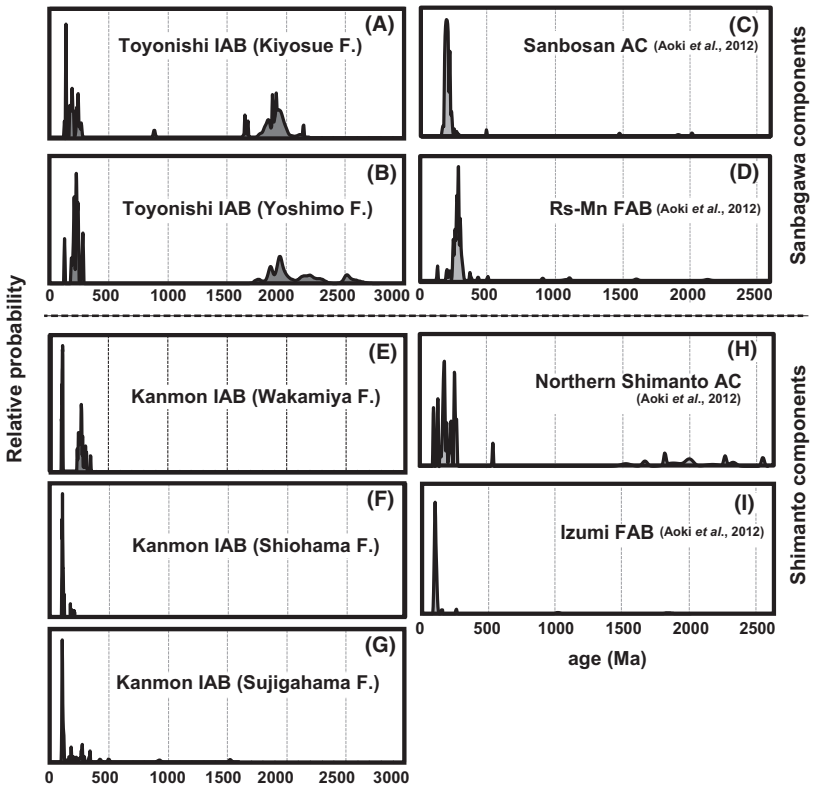

Fig. 3 (A–D) Probability age frequency curves of analysed samples from the Sanbagawa orogen. (E–I) Probability age frequency curves of analysed samples from the Shimano orogen. Some of the data are from Aoki *et al.* (2012).

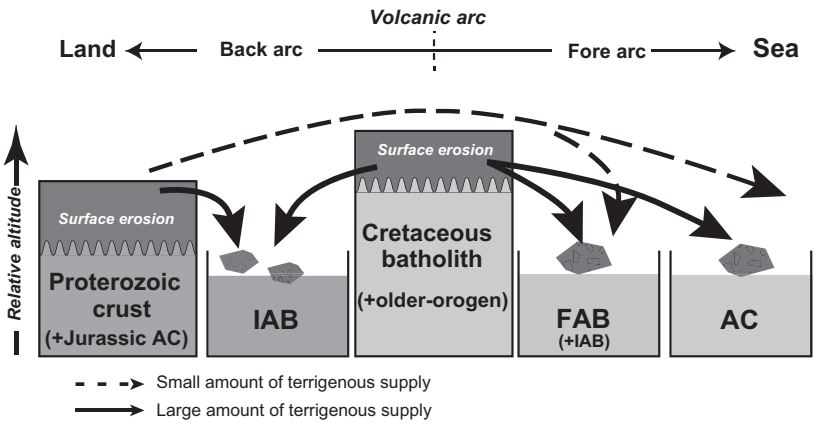

Fig. 4 Schematic illustration showing the terrigenous supply system in an orogen. Batholiths form an efficient barrier that restricts the direct delivery of clastics from the back-arc side to the fore-arc side.

orogens in Japan demonstrates that the supply of terrigenous clastics to arc-related basins was influenced by the development of a coeval arc batholith belt. Figure 5 shows a schematic cross-section of the Cretaceous arc-trench system in Japan, modelled on this study and Aoki *et al.* (2011, 2012). During the Early to Late Cretaceous orogenic processes in Japan, abundant terrigenous clastics from the Permian-Early Cretaceous arc batholiths were supplied to both the fore-arc and back-arc domains. In contrast, Proterozoic zircons originating from the Asian continent were supplied abundantly to the back-arc basins but few reached the coeval FABs. We conclude that the change in topographic relief of an arc batholith with time was critical in determining and controlling the supply routes of terrigenous clastics to arc-related basins in a Pacific-type orogen. Our results from Cretaceous Japan show that comparative analysis of zircon age spectra among arc-related basins could help to unravel the history of other older Pacific-type orogens.

Acknowledgements

K. D. Collerson assisted in English language corrections. Constructive comments by J. P. Morgan (handling editor) and three anonymous reviewers were quite helpful. This study was supported by a Research Fellowship of the Japan Society for the Promotion of Science (JSPS) for Young Scientists (23-6135 to K.A.) and a Grant-in-Aid of the JSPS (20224012 to Y.I.).

References

Aoki, K., Kitajima, K., Masago, H., Nishizawa, M., Terabayashi, M., Omori, S., Yokoyama, T., Takahata, N., Sano, Y. and Maruyama, S., 2009. Metamorphic P-T–time history of the Sanbagawa belt in central Shikoku, Japan and implications for retrograde metamorphism during exhumation. *Lithos*, **113**, 393–407.

Aoki, K., Maruyama, S., Isozaki, Y., Otoh, S. and Yanai, S., 2011. Recognition of the Shimanto HP metamorphic belt within the traditional Sanbagawa HP metamorphic belt: new perspectives of the Cretaceous–Paleogene tectonics in Japan. *J. Asian Earth Sci.*, **42**, 355–369.

Aoki, K., Isozaki, Y., Yamamoto, S., Maki, K., Yokoyama, T. and Hirata, T., 2012. Tectonic erosion in a Pacific-type orogen: Cretaceous tectonics in Japan. *Geology*, **40**, 1087–1090.

Clift, P.D., Carter, A., Draut, A.E., Long, H.V., Chew, D.M. and Schouten, H.A., 2009. Detrital U-Pb zircon dating of lower Ordovician syn-arc-continent collision conglomerates in the Irish Caledonides. *Tectonophysics*, **479**, 165–174.

Corfu, F., Hanchar, J.M., Hoskin, P.W.O. and Kinny, P., 2003. An atlas of zircon textures. In: *Zircon: Reviews in Mineralogy and Geochemistry* (J.M.

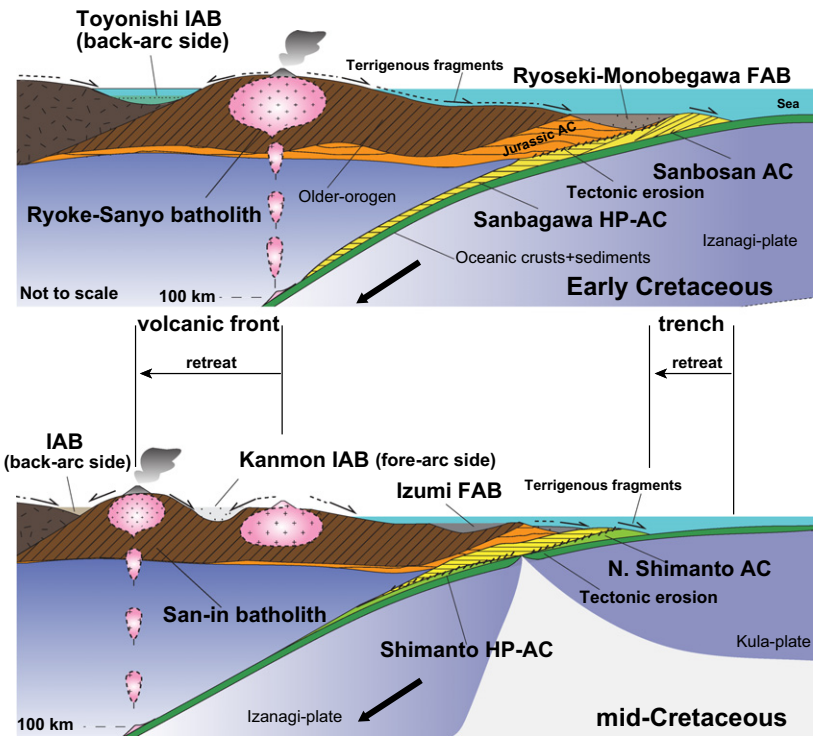

Fig. 5 Schematic cross-sections of the Cretaceous orogen in Japan showing the terrigenous supply system. The formation of the subduction-derived tonalite–trondjhemite–granodiorite granitic batholith played an important role in the control of the terrigenous supply route between the fore-arc and back-arc basins. In the subduction zone, protoliths of the mixed clastics of the Cretaceous Sanbagawa and Shimanto HP-ACs were derived from surface-eroded and tectonic-eroded crusts (Aoki *et al.*, 2012). The positions of the trench and volcanic front retreated landwards by tectonic erosion (Aoki *et al.*, 2011, 2012).

Hanchar and P.W.O. Hoskin, eds). *Mineral. Soc. Am.*, **53**, 469–500.
Darby, B.J. and Gehrels, G., 2006. Detrital zircon reference for the North China block. *J. Asian Earth Sci.*, **26**, 637–648.
Dickinson, W.R. and Gehrels, G.E., 2008a. U-Pb ages of detrital zircons in relation to paleogeography: Triassic paleodrainage networks and sediment dispersal across southwest Laurentia. *J. Sed. Res.*, **78**, 745–764.
Dickinson, W.R. and Gehrels, G.E., 2008b. Sediment delivery to the Cordilleran foreland basin: insights from U-Pb ages of detrital zircons in Upper Jurassic and Cretaceous strata of the Colorado Plateau. *Am. J. Sci.*, **308**, 1041–1082.
Dickinson, W.R. and Rich, E.I., 1972. Petrologic intervals and petrofacies in the Great Valley Sequence, Sacramento Valley, California. *Geol. Soc. Am. Bull.*, **83**, 3007–3024.
Dickinson, W.R. and Suczek, C.A., 1979. Plate tectonics and sandstone compositions. *Am. Assoc. Petrol. Geol. Bull.*, **63**, 2164–2182.
Dickinson, W.R., Ingersoll, R.V., Cowan, D.S., Helmold, K.P. and Suczek, C.A., 1982. Provenance of Franciscan graywackes in coastal California. *Geol. Soc. Am. Bull.*, **93**, 95–107.
Dickinson, W.R., Beard, L.S., Brackenridge, G.R., Erjavec, J.L., Ferguson, R.C., Inman, K.F., Knepp, R.A., Lindberg, F.A. and Ryberg, P.T., 1983. Provenance of North American Phanerozoic sandstones in relation to tectonic setting. *Geol. Soc. Am. Bull.*, **94**, 222–235.
Dumitru, T.A., Wakabayashi, J., Wright, J.E. and Wooden, J.L., 2010. Early Cretaceous transition from nonaccretionary behavior to strongly accretionary behavior within the Franciscan subduction complex. *Tectonics*, **29**, TC5001.
Gehrels, G.E., Dickinson, W.R., Darby, B.J., Harding, J.P., Manuszak, J.D., Riley, B.C.D., Spurlin, M.S., Finney, S.C., Girty, G.H., Harwood, D.S., Miller, M.M., Satterfield, J.I., Smith, M.T., Snyder, W.S., Wallin, E.T. and Wyld, S.J., 2000. Tectonic implications of detrital zircon data from Paleozoic and Triassic strata in western Nevada and northern California. In: *Paleozoic and Triassic Paleogeography and Tectonics of Western Nevada and Northern California* (M.J. Soreghan and G.E. Gehrels, eds). *Geol. Soc. Am. Spec. Pap.*., **347**, 133–150.
Hirata, T., Iizuka, T. and Orihashi, Y., 2005. Reduction of mercury background on ICP-mass spectrometry for in situ U-Pb age determinations of zircon samples. *J. Anal. At. Spectrom.*, **20**, 696–701.
Iizuka, T. and Hirata, T., 2004. Simultaneous determinations of U-Pb age and REE abundance for zircons using ArF excimer laser ablation-ICPMS. *Geochem. J.*, **38**, 229–241.
Iizumi, S., Sawad, Y., Sakiyama, T. and Imaoka, T., 1985. Cretaceous to Paleogene magmatism in the Chugoku and Shikoku Districts, Japan. *Earth Sci. (Chikyu Kagaku)*, **39**, 372–384. (in Japanese with English abstract).
Isozaki, Y., 1996. Anatomy and genesis of a subduction-related orogen: a new view of geotectonic subdivision and evolution of the Japanese Islands. *Island Arc*, **5**, 289–320.
Isozaki, Y., Aoki, K., Nakama, T. and Yanai, S., 2010. New insight into a subduction-related orogen: reappraisal on geotectonic framework and evolution of the Japanese Islands. *Gondwana Res.*, **18**, 82–105.
Isozaki, Y., Maruyama, S. and Furuoka, F., 1990. Accreted oceanic materials in Japan. *Tectonophysics*, **181**, 179–205.
Jaffey, A.H., Flynn, K.F., Glendenin, L.E., Bentleyt, W.C. and Essling, A.M., 1971. Precision measurement of half-lives and specific activities of ^{235}U and ^{238}U. *Phys. Rev. C*, **4**, 1889–1906.
Jin, W., 2002. The late Paleoproterozoic orogeny in the North China craton. *Gondwana Res.*, **5**, 95–99.
LaMaskin, T.A., 2012. Detrital zircon facies of Cordilleran terranes in western North America. *GSA Today*, **22**, 4–11.
Liu, X., Gao, S., Diwu, C. and Ling, W., 2008. Precambrian crustal growth of Yangtze craton as revealed by detrital zircon studies. *Am. J. Sci.*, **308**, 421–468.
Ludwig, K., 2003. *Isoplot 3.0*. A geochronological toolkit for Microsoft Excel. Berkeley Geochronology Center Special Publication 4, CA, 70 pp.
Maruyama, S., 1997. Pacific-type orogeny revisited: Miyashiro-type orogeny proposed. *Island Arc*, **6**, 91–120.
Maruyama, S., Liou, J.G. and Seno, T., 1989. Mesozoic and Cenozoic evolution of Asia. In: *The Evolution of the Pacific Ocean Margins* (Z. Ben-Avraham, ed.), pp. 75–99. Oxford University Press, New York.
Maruyama, S., Liou, J.G. and Terabayashi, M., 1996. Blueschists and eclogites of the world and their exhumation. *Int. Geol. Rev.*, **38**, 485–594.

Maruyama, S., Isozaki, Y., Kimura, G. and Terabayashi, M., 1997. Paleogeographic maps of the Japanese Islands: plate tectonics synthesis from 750 Ma to the present. *Island Arc*, **6**, 121–141.

Matsuda, T. and Ueda, S., 1971. On the Pacific-type orogeny and its model: exhumation of the paired metamorphic belts concept and possible origin of marginal seas. *Tectonophysics*, **11**, 5–27.

Matsumoto, T., 1949. The late Mesozoic geological history in the Nagato Province, Southwest Japan. *J. Geol. Geogr.*, **21**, 235–224.

Matsumoto, T., 1951. The Yezo Group and the Kwanmon Group. *J. Geol. Soc. Japan*, **57**, 95–98. (in Japanese with English abstract).

Miyata, T., 1980. Wrench fault tectonics of the Median Tectonic Line and deformation of the Cretaceous Izumi Group in west Kinki, southwest Japan. *J. Geosci., Osaka City University*, **23**, 65–114.

Nakajima, T., Shirahase, T. and Shibata, K., 1990. Along-arc lateral variation of Rb-Sr and K-Ar ages of Cretaceous granitic rocks in Southwest Japan. *Contrib. Mineral. Petrol.*, **104**, 381–389.

Nutman, A.P., Sano, Y., Terada, K. and Hidaka, H., 2006. 743 ± 17 Ma granite clast from Jurassic conglomerate, Kamiaso, Mino Terrane, Japan: the case for South China Craton provenance (Korean Gyeonggi Block?). *J. Asian Earth Sci.*, **26**, 99–104.

Shibata, K. and Adachi, M., 1974. Rb-Sr whole-rock ages of Precambrian metamorphic rocks in the Kamiaso conglomerate from central Japan. *Earth Planet. Sci. Lett.*, **21**, 277–287.

Sláma, J., Košler, J., Condon, D.J., Crowley, J.L., Gerdes, A., Hancharg, J.M., Horstwood, M.S.A., Morris, G.A., Nasdala, L., Norberg, N., Schaltegger, U., Schoene, B., Tubrett, M.N. and Whitehouse, M.J., 2008. Plesovice zircon – a new natural reference material for U-Pb and Hf isotopic microanalysis. *Chem. Geol.*, **249**, 1–35.

Suzuki, H., Isozaki, Y. and Itaya, T., 1990. Tectonic superposition of the Kurosegawa terrane upon the Sanbagawa metamorphic belt in eastern Shikoku, Southwest Japan–K-Ar ages of weakly metamorphosed rocks in northeastern Kamikatsu Town, Tokushima Prefecture. *J. Geol. Soc. Japan*, **6**, 143–153. (in Japanese with English abstract).

Suzuki, K., Adachi, M. and Tanaka, T., 1991. Middle Precambrian provenance of Jurassic sandstone in the Mino Terrane, central Japan: Th–U–total Pb evidence from an electron microprobe monazite study. *Sed. Geol.*, **75**, 141–147.

Uyeda, S. and Miyashiro, A., 1974. Plate tectonics and the Japanese Islands: a synthesis. *Geol. Soc. Am. Bull.*, **85**, 1159–1170.

Wang, Y., Zhang, F., Fan, W., Zhang, G., Chen, S., Cawood, P.A. and Zhang, A., 2010. Tectonic setting of the South China Block in the early Paleozoic: resolving intracontinental and ocean closure models from detrital zircon U–Pb geochronology. *Tectonics*, **29**, TC6020.

Wiedenbeck, M., Alle, P., Corfu, F., Griffin, W.L., Meier, M., Oberli, F., van Quadt, A., Roddick, J.C. and Spiegel, W., 1995. Three natural zircon standards for U-Th-Pb, Lu-Hf, trace element and REE analyses. *Geostandards Newslett.*, **19**, 1–23.

Wiedenbeck, M., Hanchar, J.M., Peck, W.H., Sylvester, P., Valley, J., Whitehouse, M., Kronz, A., Morishita, Y., Nasdala, L., Fiebig, J., Franchi, I., Girard, J.P., Greenwood, R.C., Hinton, R., Kita, N., Mason, P.R.D., Norman, M., Ogasawara, M., Piccoli, P.M., Rhede, D., Satoh, H., Schulz-Dobrick, D., Skår, Ø., Spicuzza, M.J., Terada, K., Tindle, A., Togashi, S., Vennemann, T., Xie, Q. and Zheng, Y.-F., 2004. Further characterisation of the 91500 zircon crystal. *Geostand. Geoanal. Res.*, **28**, 9–39.

Xu, X., Xue, D., Li, Y., Hu, P. and Chen, N., 2014. Neoproterozoic sequences along the Dexing–Huangshan fault zone in the eastern Jiangnan orogen, South China: geochronological and geochemical constrains. *Gondwana Res.*, **25**, 368–382.

Yamada, T. and Ohno, T., 2005. Revision of the stratigraphy of the Toyora and Toyonishi Groups in the Ouchi-Kikugawa area, Yamaguchi Prefecture, west Japan. *J. Geol. Soc. Japan*, **111**, 389–403.

Yamamoto, A., Tanabe, K. and Isozaki, Y., 2009. The Lower Cretaceous fresh-water stromatolites in northern Kyushu, Japan. *Paleontol. Res.*, **13**, 139–149.

Yoshidomi, K., 2009. Toyonishi Group and Kanmon Group. In: *Regional Geology of Japan, Part 6, Chugoku district* (Y. Nishimura, ed.), pp. 100–105. Asakura, Tokyo, (in Japanese).

Zhu, X.-Q., Zhu, W.-B., Ge, R.-F. and Wang, X., 2014. Late Paleozoic provenance shift in the south-central North China Craton: implications for tectonic evolution and crustal growth. *Gondwana Res.*, **25**, 383–400.

Received 8 April 2013; revised version accepted 7 October 2013

